Supporting Information

Transparent photoactuators based on localized-surface-plasmon-resonant semiconductor nanocrystals: a platform for camouflage soft robots

Feng Huang[a,c,d], Mingcen Weng[a,c,d], Zhuohong Feng[a,c,d], Xiao Li[b], Wei Zhang[a,c,d,*], Luzhuo Chen[a,c,d,*]

[a] Fujian Provincial Key Laboratory of Quantum Manipulation and New Energy Materials, College of Physics and Energy, Fujian Normal University, Fuzhou, 350117, China.

[b] Key Laboratory of Design and Assembly of Functional Nanostructures, Fujian Institute of Research on the Structure of Matter, Chinese Academy of Sciences, University of Chinese Academy of Sciences, Fuzhou, 350002, China.

[c] Fujian Provincial Collaborative Innovation Center for Advanced High-Field Superconducting Materials and Engineering, Fuzhou, 350117, China.

[d] Fujian Provincial Engineering Technology Research Center of Solar Energy Conversion and Energy Storage, Fuzhou, 350117, China.

*E-mail: chenluzhuo@163.com, wzhang721@163.com

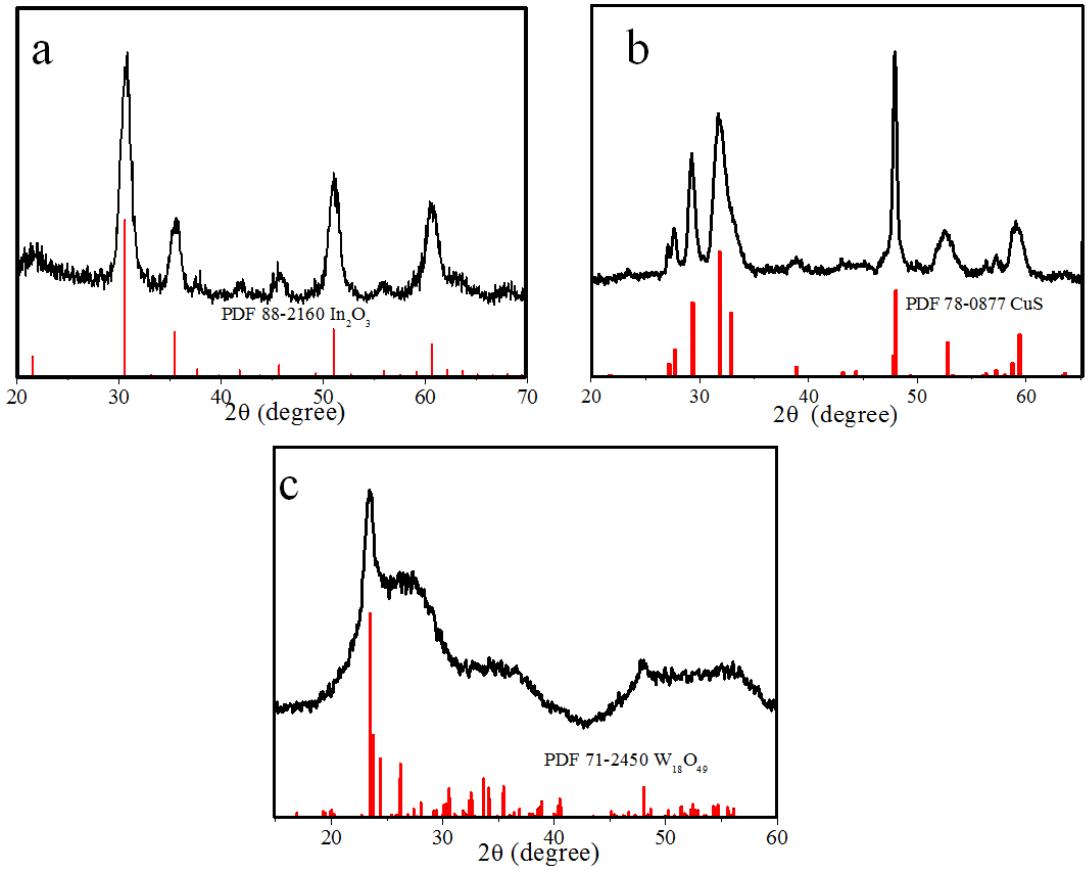

Fig. S1. XRD patterns for the synthesized nanocrystals. (**A**) ITO. (**B**) CuS. (**C**) $W_{18}O_{49}$. Bars on the bottoms are the standard data for the cubic In_2O_3 (PDF 88-2160), Cubic CuS (PDF 78-0877) and monoclinic $W_{18}O_{49}$ (PDF 71-2450).

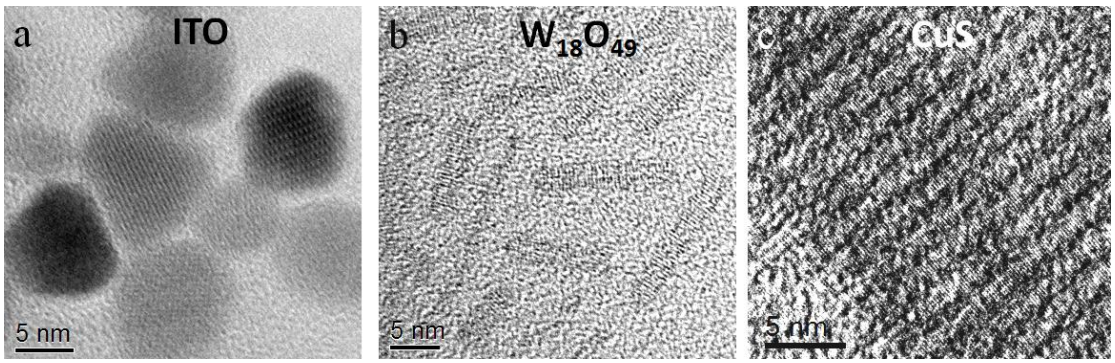

Fig. S2. HRTEM images of the synthesized ITO, $W_{18}O_{49}$ and CuS nanocrystals.

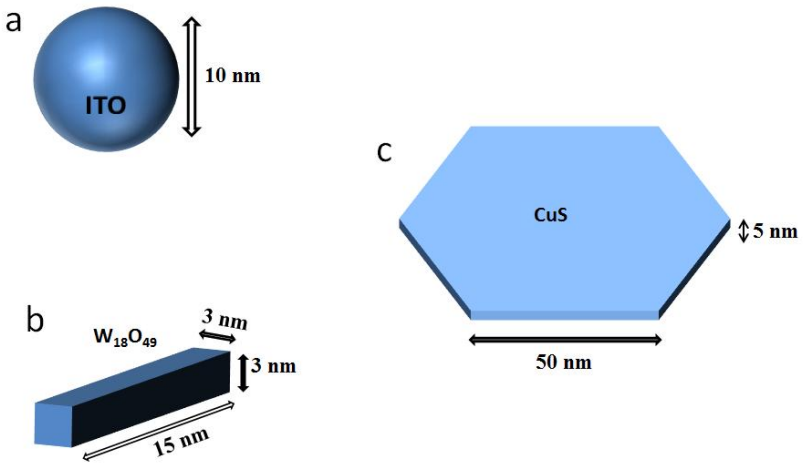

Fig. S3. The models of ITO, $W_{18}O_{49}$ and CuS nanocrystals established for FDTD simulation.

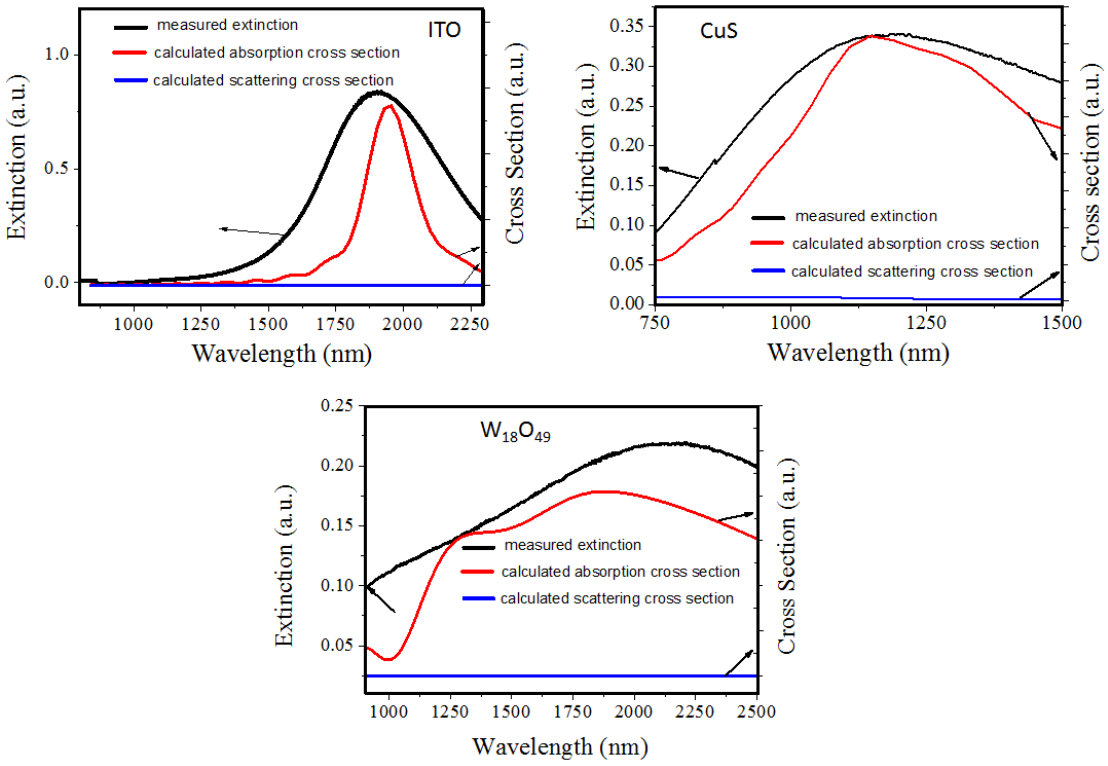

Fig. S4. FDTD simulated absorption/scattering cross sections for ITO, $W_{18}O_{49}$ and CuS nanocrystals, accompanied with the measured extinction spectra.

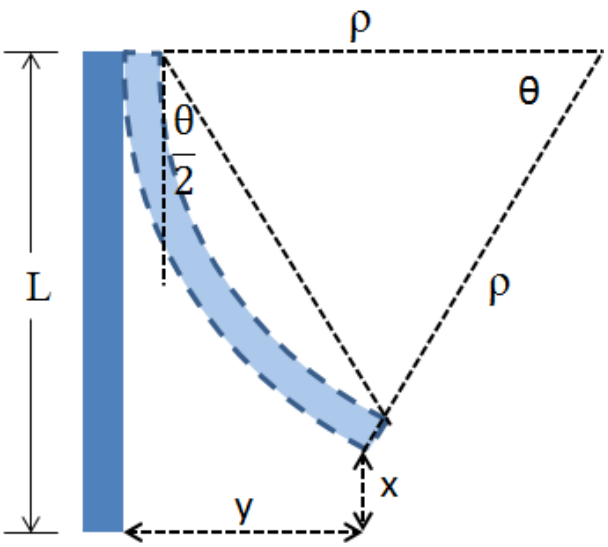

Fig. S5. Schematic illustration for the calculation principle of bending curvature from length and bending angle of the actuator.

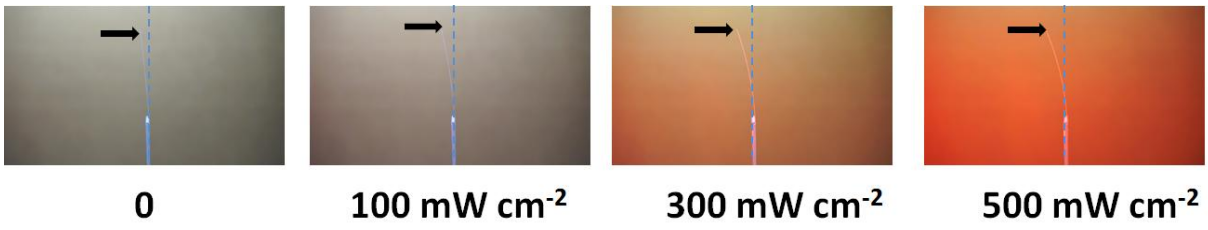

Fig. S6. Photographs displaying the behavior of the BOPP/PET film upon NIR light irradiation.

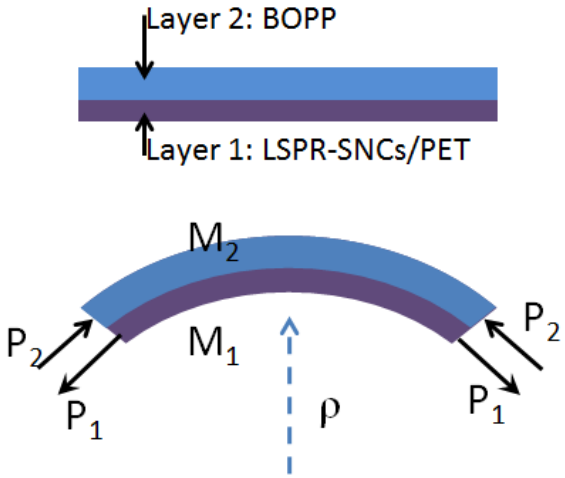

Fig. S7. Schematic illustration of the bilayer configurational actuation model.

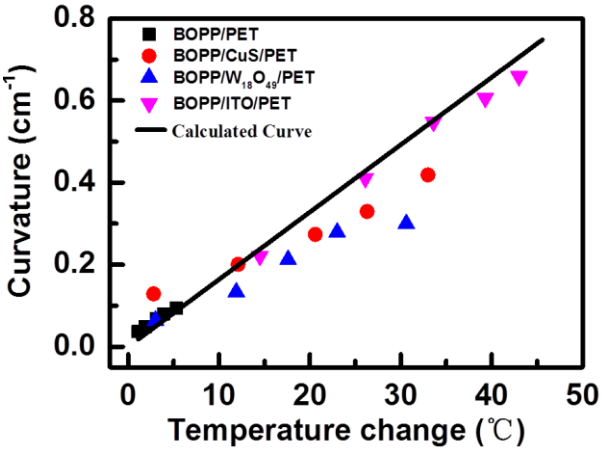

Fig. S8. Calculated curvature as a function of temperature change for the BOPP-PET actuation system. The data of the BOPP/LSPR-SNCs/PET actuators is also presented for comparison.

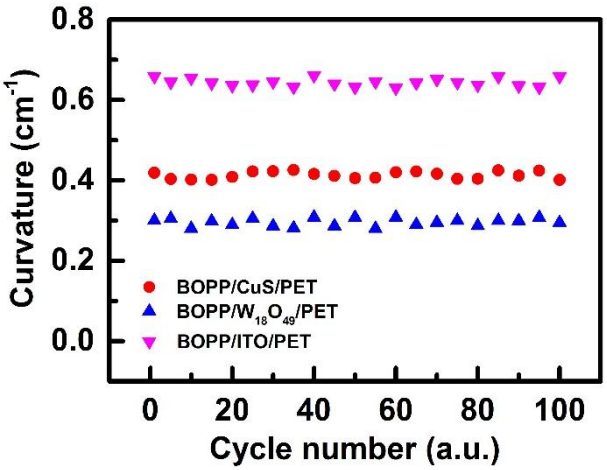

Fig. S9. Repeatability test results of the NIR light-driven actuation of the BOPP/LSPR-SNCs/PET actuators.

Fig. S10. Ratchet-shaped substrate for worm-like crawling robot.

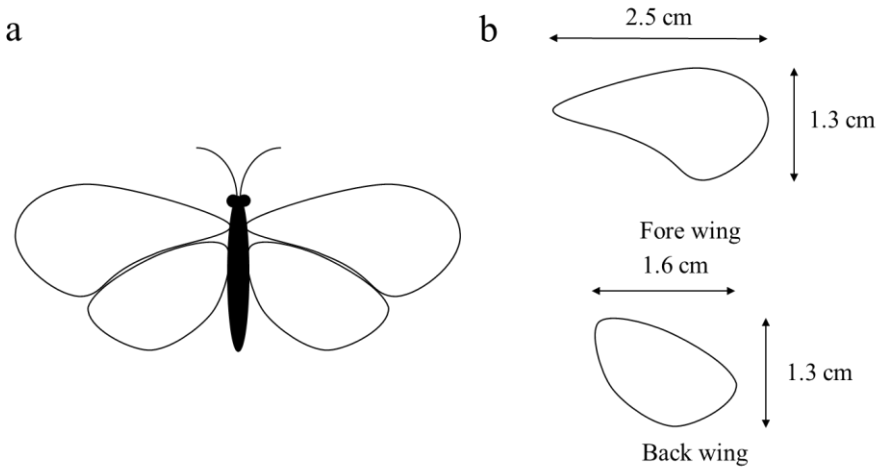

Fig. S11. Structure of the glasswing butterfly robot.

Note S1: Finite different time domain (FDTD) calculation for estimating the absorption and scattering of ITO, $W_{18}O_{49}$ and CuS nanocrystals

1. Permittivity of ITO, $W_{18}O_{49}$ and CuS

To perform FDTD model, first of all, the permittivity of ITO, $W_{18}O_{49}$ and CuS should be estimated. Herein, we employ Drude mode to estimate the permittivity of these materials, which can be written as:

$$\varepsilon = 1 - \frac{\omega_p^2}{\omega^2 + i\gamma\omega} \quad \text{(S1)}$$

where ω_p is the bulk plasma frequency, while γ is the collision frequency term. According to the previous work, for the ITO material, the ω_p is 1.89×10^{15} rad s^{-1}, while γ is 9.72×10^{13} rad s^{-1},[S1] for the $W_{18}O_{49}$ material, the ω_p is 3.15×10^{15} rad s^{-1}, while γ is 4.86×10^{14} rad s^{-1},[S2] and for the CuS material the ω_p is 2.3×10^{15} rad s^{-1}, while γ is 2.24×10^{14} rad s^{-1}.[S3] Substituting these parameters into Equation (S1), the permittivity of ITO, $W_{18}O_{49}$ and CuS can be obtained.

2. Morphology Model of ITO, $W_{18}O_{49}$ and CuS Nanocrystals

The morphology models to be simulated for the ITO, $W_{18}O_{49}$ and CuS are presented in Fig. S3. The model for ITO is a sphere with the diameter of 10 nm. For $W_{18}O_{49}$, we establish a model of tetragonal rod, with the length of 15 nm and the width of 3 nm. As for CuS, the established model is a hexagonal plate with the diameter of 100 nm and the thickness of 5 nm.

3. Calculation Method

We used a commercial software package, FDTD Solutions, developed by Lumerical Solutions, Inc., to investigate the decay behavior of a dipole emitter in the vicinity of a nanoparticle. The refractive index of the surrounding medium is considered non-dispersive and

equal to 1.4 for cyclohexane. The simulation domain is enclosed by perfectly matched layers (PMLs) to absorb the outward propagating radiation. In the electromagnetic treatment, the far-field radiation power from the dipole source are collected by integrating the Poynting vector over the surface of a virtual box placed 500 nm away from the dipole. The total radiation power from the dipole is collected by integrating the Poynting vector over the whole surface of an inner small box that just encloses the dipole. In addition, the 3D-FDTD mesh discretization around the dipole is chosen to be 1 nm.

4. Calculation Results and Discussion

Fig. S4 displays the calculated LSPR absorption/scattering cross-sections as the function of the incident wavelength. For comparison, the measured extinction spectra were also presented. There is more or less mismatch between the measured data and the calculated results, as the morphology of the practical synthesized nanocrystals do not uniformly consist with the morphology model established for FDTD simulation. Nevertheless, the results confirm that for these nanocrystals, the LSPR extinctions are majorly composed of absorption behavior.

Note S2: Bending curvature calculation principle for the actuators

The parameters are defined as follows (shown in Fig. S5):

L: The length of the actuator.

ρ: The radius of the arc of the curved actuator.

x: The horizontal free-end displacement of the actuator.

y: The vertical free-end displacement of the actuator.

$\theta/2$: The chord tangent angle of the actuator.

θ: The bending angle of the arc of the actuator.

The curvature is defined as the reciprocal radius ($1/\rho$).

The chord tangent angle is given by

$$\frac{\theta}{2} = \arctan\frac{x}{y} \tag{S2}$$

As the bending angle is given by

$$\theta = \frac{L}{\rho}, \tag{S3}$$

the curvature $1/\rho$ is deduced as

$$\frac{1}{\rho} = \frac{\theta}{L}. \tag{S4}$$

Hence, the bending curvature of the actuator can be calculated by achieving the bending angle and length of the actuator.

Note S3: A bilayer configurational model for theoretically calculating the curvature of BOPP/LSPR-SNCs/PET actuators

Herein, BOPP/LSPR-SNCs/PET actuator is approximated to a bilayer configuration, composed of LSPR-SNCs/PET layer (Layer 1) and BOPP layer (Layer 2). When the temperature decreases, the actuator bends towards PET side due to the relatively large CTE of BOPP. Since the actuator is bending, all forces acting over the cross-section of layer 1 can be represented as an axial tensile force (P_1) and bending moment (M_1). On the other side, axial compressive force (P_2) and bending moment (M_2) are acting in the cross-section of Layer 2, as illustrated in Fig. S7. Because no external forces are acting on the actuator, all internal forces acting on cross-section of the bilayer structure should be in equilibrium. Hence,

$$P = P_1 = P_2, \tag{S5}$$

$$\left(\frac{t_1+t_2}{2}\right)P = M_1 + M_2. \tag{S6}$$

From the beam theory,

$$M_1 = \frac{E_1 I_1}{\rho},\ M_2 = \frac{E_2 I_2}{\rho},\ I_1 = \frac{bt_1^3}{12} \text{ and } I_2 = \frac{bt_2^3}{12} \tag{S7}$$

where ρ is the radius of the curved actuator, E_1 and E_2 are Young's modules of Layer 1 and Layer 2, respectively, I_1 and I_2 are the moment of inertia for Layer 1 and Layer 2, b is the width of the actuator, and t_1 and t_2 are the thickness of Layer 1 and Layer 2, respectively. By substituting M_1 and M_2 into Equation (S6), we have:

$$\left(\frac{t_1+t_2}{2}\right)P = \frac{E_1 I_1}{\rho} + \frac{E_2 I_2}{\rho} \tag{S8}$$

On the other hand, the normal strain is the same at the interface of Layer 1 and Layer 2. Considering that, the normal strain is the sum of strains caused by the axial force (P), bending of the actuator, thermal expansion of Layer 1 and Layer 2. We have:

$$\varepsilon_1 + \frac{t_1}{2\rho} + \frac{P}{E_1 t_1 b} = \varepsilon_2 - \frac{t_2}{2\rho} - \frac{P}{E_2 t_2 b} \quad \text{(S9)}$$

where ε_1 and ε_2 are thermal expansive strains of Layer 1 and Layer 2, and can be express as: $\varepsilon_1 = \alpha_1 \Delta T$, $\varepsilon_2 = \alpha_2 \Delta T$ (α_1 and α_2 are the CTE of Layer 1 and Layer 2, respectively. ΔT is the temperature change).

Combining Equation (S9) with Equation (S8) to substitute *P* value, we have:

$$\frac{1}{\rho} = \frac{6E_1E_2t_1t_2(t_1+t_2)(\alpha_2\Delta T - \alpha_1\Delta T)}{(E_1t_1^2)^2 + (E_2t_2^2)^2 + 2E_1E_2t_1t_2(2t_1^2 + 3t_1t_2 + 2t_2^2)} \quad \text{(S10)}$$

Herein, Layer 1 (LSPR-SNCs/PET layer) is a composited layer. However, since the thickness of LSPR-SNCs is much smaller than PET, we assume that the Young's module of Layer 1 (E_1) is approximatively equal to the Young's modules of PET.

Substituting the value of Young's modules (E_1=2.6 GPa, E_2=1.1 GPa) and thickness of each layer (t_1 = 5 μm + 25 μm = 30 μm, t_2 = 40 μm), the bending curvature ($1/\rho$) as a function of temperature changes can be calculated, which have been presented in Fig. S8.

Supporting references:

S1. Laux, S, Kaiser, N, Zöller, A, Götzelmann, R, Lauth, H, Bernitzki, H, *Appl. Optics* **2008**, *47*, C297.

S2. Viswanathan, K, Brandt, K, Salje, E, *J. Solid State Chem.* **1981**, *36*, 45.

S3. Wei, T, Liu, Y, Dong, W, Zhang, Y, Huang, C, Sun, Y, Chen, X, Dai, N, *Appl. Mater. & Interfaces* **2013**, *5*, 10473.

Supporting Movies

Movie S1: Crawling motion of a worm-like robot.

Movie S2: A glasswing butterfly robot driven by infrared light.

Movie S3: A two-finger robot hand driven by infrared light.